PNAS INAUGURAL ARTICLE | CELL BIOLOGY OPEN ACCESS

The cGAS–STING, p38 MAPK, and p53 pathways link genome instability to accelerated cellular senescence in ATM-deficient murine lung fibroblasts

Majd Haj[a], Yann Frey[a], Amit Levon[a], Avishai Maliah[a], Tal Ben-Yishay[a], Rachel Slutsky[a], Riham Smoom[b], Yehuda Tzfati[b], Uri Ben-David[a], Carmit Levy[a], Ran Elkon[a], Yael Ziv[a], and Yosef Shiloh[a,1]

Affiliations are included on p. 10.

This contribution is part of the special series of Inaugural Articles by members of the National Academy of Sciences elected in 2023.
Contributed by Yosef Shiloh; received September 19, 2024; accepted December 5, 2024; reviewed by Aaron Ciechanover and Moshe Oren

Ataxia–telangiectasia (A-T) is a pleiotropic genome instability syndrome resulting from the loss of the homeostatic protein kinase ATM. The complex phenotype of A-T includes progressive cerebellar degeneration, immunodeficiency, gonadal atrophy, interstitial lung disease, cancer predisposition, endocrine abnormalities, chromosomal instability, radiosensitivity, and segmental premature aging. Cultured skin fibroblasts from A-T patients exhibit premature senescence, highlighting the association between genome instability, cellular senescence, and aging. We found that lung fibroblasts derived from ATM-deficient mice provide a versatile experimental system to explore the mechanisms driving the premature senescence of primary fibroblasts lacking ATM. *Atm*−/− fibroblasts failed to proliferate under ambient oxygen conditions (21%). Although they initially proliferated under physiological oxygen levels (3%), they rapidly entered senescence. In contrast, wild-type (WT) lung fibroblasts did not senesce under 3% oxygen and eventually underwent immortalization and neoplastic transformation. However, rapid senescence could be induced in WT cells either by *Atm* gene ablation or persistent chemical inhibition of ATM kinase activity, with senescence induced by ATM inhibition being reversible upon inhibitor removal. Moreover, the concomitant loss of ATM and p53 led to senescence evasion, vigorous growth, rampant genome instability, and subsequent immortalization and transformation. Our findings reveal that the rapid senescence of *Atm*−/− lung fibroblasts is driven by the collaborative action of the cGAS–STING, p38 MAPK, and p53 pathways in response to persistent DNA damage, ultimately leading to the induction of interferon-α1 and downstream interferon-stimulated genes. We propose that accelerated cellular senescence may exacerbate specific A-T symptoms, particularly contributing to the progressive, life-threatening interstitial lung disease often observed in A-T patients during adulthood.

ataxia–telangiectasia | ATM | senescence | p53 | cGAS-STING

Significance

Understanding the multifaceted genetic disorder ataxia–telangiectasia (A-T) offers new insights into the functions of the ATM protein kinase, the loss of which underlies this disease. A-T exemplifies the connection between genome instability, cellular senescence, and aging. This study elucidates the pathways leading to a hallmark of A-T's cellular phenotype: the premature senescence of primary fibroblasts derived from affected individuals. Our findings provide a mechanistic understanding of how inherited genome instability accelerates cellular senescence, offering potential explanations for several A-T symptoms. The work introduces murine primary lung fibroblasts growing under 3% oxygen as a valuable experimental system to explore the genome instability-senescence link and the molecular events leading to the neoplastic transformation of primary diploid cells without any directed manipulations.

Understanding the molecular and physiological foundations of rare genetic disorders is crucial for advancing therapeutic strategies and unlocking new biomedical insights, which often implicate on a broader range of diseases. Noteworthy among these are genome instability disorders, which are situated at the crossroads of genome dynamics and cellular metabolism. These disorders usually arise from deficiencies in DNA damage management, and their complex phenotypes typically include combinations of chromosomal instability, progressive degeneration of specific tissues, impaired development and/or growth, skeletal and endocrinological abnormalities, segmental premature aging, cancer predisposition, and increased sensitivity to specific DNA damaging agents (1).

The cellular system impacted in genome instability syndromes is the DNA damage response (DDR)—a complex signal transduction network that coordinates lesion-specific DNA repair pathways while modulating many physiological processes in a coordinated manner (2). This system remains continuously active, responding to DNA damage induced primarily by endogenous reactive oxygen species (ROS) as well as by environmental chemicals and radiations (3). Maintenance of genome stability against this constant offensive is essential for preventing undue cell death or the development of cancer (4).

The autosomal recessive disorder, ataxia–telangiectasia (A-T), stands as a prominent example of a genome instability disorder (5). It is caused by null mutations in the *ATM* (A-T, mutated) gene, which was identified in our lab (6) and encodes the homeostatic protein kinase, ATM (7, 8). A-T is characterized by progressive cerebellar degeneration resulting in severe motor dysfunction, oculocutaneous telangiectasia (dilated blood

We dedicate this work to the memory of our dear friend and cherished colleague, Dr. Judy Campisi (1948–2024), a true pioneer in the field of cell senescence. Her generosity and expertise were instrumental in guiding our lab into this field, particularly through her dedicated mentorship of the first author during his time in her lab. Her contributions to science and her unique personality will always remain with us.

[1]To whom correspondence may be addressed. Email: yossih@tauex.tau.ac.il.

This article contains supporting information online at https://www.pnas.org/lookup/suppl/doi:10.1073/pnas.2419196122/-/DCSupplemental.

Published January 7, 2025.

vessels), immunodeficiency often accompanied by recurrent sinopulmonary infections, interstitial lung disease that is independent of the recurrent infections, thymic and gonadal atrophy, occasional endocrine abnormalities, chromosomal instability, predisposition to cancer—primarily to lymphoreticular malignancies, and acute sensitivity to ionizing radiation (5). Notably, segmental premature aging is frequently observed in affected adolescents (9). Cultured cells derived from affected individuals exhibit chromosomal instability and cellular hypersensitivity to genotoxic agents, particularly those that induce DNA double-strand breaks (DSBs) (5, 10). Furthermore, primary fibroblasts derived from A-T patients undergo enhanced telomere erosion and accelerated replicative senescence (9, 11–13).

The ATM protein that is absent or inactivated in individuals with A-T is a pivotal serine-threonine kinase that is involved in many homeostatic pathways (7, 8). Its most studied function is orchestrating the DDR in response to DSBs: Following its activation by this DNA lesion (14–16), it phosphorylates a multitude of substrates within an intricate, highly structured signaling web (17–19). ATM is also involved in responding to other types of DNA lesions (20, 21), and is additionally triggered by ROS, underscoring its importance in the cellular defense against oxidative stress (8). Moreover, ATM is implicated in the regulation of mitochondrial homeostasis and several other cellular metabolic circuits (7, 8). Consequently, the multifaceted clinical and cellular phenotypes observed in A-T can be attributed to the simultaneous loss of these functions (8). Nonetheless, ongoing efforts still aim to link the loss of individual ATM functions to particular A-T symptoms and cellular characteristics.

DDR deficits have been robustly associated with accelerated aging (22) and A-T is no exception (9, 23). The role of premature aging in exacerbating A-T symptoms likely becomes more pronounced as affected individuals age. A common feature of aging tissues is the accumulation of senescent cells (24–26). Premature senescence of specific cell types may thus be a mediator of the segmental premature aging observed in A-T. The accelerated senescence observed in A-T primary fibroblast lines (9, 11–13) may be indicative of such a phenomenon.

Cellular senescence is characterized by persistent cell cycle arrest, apoptosis resistance, significant morphological changes, metabolic alterations, chromatin organization shifts, epigenomic and gene expression modifications, and, increased basal DNA damage (27). Replicative senescence, initially identified in cultured primary fibroblast lines (28), has been associated with telomere erosion (28). However, cellular senescence can also be triggered by various stresses such as genotoxic stress, oncogene activation, and others (27, 29). These signals usually affect pathways that converge at the activation of the p53-p21 and p16-RB axes, acting as cell cycle regulators that prevent the proliferation of damaged or stressed cells.

Senescent cells are also characterized by the senescence-associated secretory phenotype (SASP), which involves extensive release of bioactive molecules, many of them inflammatory, with autocrine and paracrine effects (26, 27). While the SASP can exert beneficial effects in specific contexts (30), its extended presence may lead to persistent tissue damage and foster a localized, chronic inflammatory microenvironment eventually leading to tissue aging (26, 31). Cellular senescence therefore is a double-edged sword: It is crucial for embryonic development, tissue repair, removal of damaged cells, and tumor suppression. However, over time, it can also promote inflammation, accelerate degenerative diseases, contribute to cancer progression, and intensify aging-related conditions.

Given the role of ATM in regulating the cellular redox balance, we recently asked whether reducing oxygen concentration into the physiological range could attenuate the accelerated senescence observed in cultured A-T skin fibroblasts. Remarkably, at 3% oxygen, the lifespan of these cells until reaching senescence was significantly prolonged. However, they still senesced earlier than control cells grown under identical conditions (13). Transcriptomic analysis revealed that the accelerated senescence in A-T fibroblasts predominantly manifested as replicative senescence, albeit with distinct transcriptomic signatures. Notably, we observed the activation of SASP genes in senescing A-T cells, whose products had been reported to be involved in tissue fibrosis. This observation resonates with the development of interstitial lung disease in affected individuals advancing in age (32), a condition that may be exacerbated by chemotherapy (33).

Understanding the underlying causes and cellular pathways responsible for the premature senescence observed in ATM-deficient fibroblasts holds significant implications both in basic research and for clinical practice. In our recent study of A-T cell lines, we noticed a high level of micronuclei (MN) in these cells, along with concomitant activation of interferon-stimulated genes (ISGs) (13). Expanding upon these findings, we aimed to utilize a cellular system that would demonstrate the premature senescence of ATM-deficient cells more rapidly compared to human skin fibroblasts and would be conveniently amenable to further experimental manipulations. Given the association of fibrotic lung disease with A-T, we found that ATM-deficient, murine primary lung fibroblast lines indeed met these criteria.

Results

Rapid Senescence of Murine *Atm−/−* Lung Fibroblasts at Physiological Oxygen Concentrations. Primary lung fibroblasts from wild-type (WT) and *Atm*−/− mice were cultured under ambient (21%) or 3% oxygen concentrations. Under ambient conditions, WT cells senesced within several passages, exhibiting senescence characteristics and DNA damage indicators, such as nuclear foci of phosphorylated histone H2AX (γH2AX) and MN (*SI Appendix*, Fig. S1). These observations are similar to those seen in senescing mouse embryo fibroblasts (MEFs) (34), suggesting that the growth of WT mouse primary fibroblasts is limited under these conditions. Establishing cultures of *Atm*−/− fibroblasts under ambient conditions was unsuccessful. In contrast, at 3% O_2, WT cells accumulated less DNA damage (Fig. 1 and *SI Appendix*, Fig. S1) and demonstrated robust growth without any signs of senescence for at least 35 passage levels (*SI Appendix*, Fig. S3). This suggests eventual immortalization, similarly to MEFs growing under 3% O_2 (34, 35). Importantly, at this oxygen level, *Atm*−/− fibroblast lines could be initiated, but they exhibited significantly slower growth compared to WT cells, and consistently halted at passage level 8 (P8) (Fig. 1 and *SI Appendix*, Figs. S1 and S2). At this stage, they displayed distinctive senescence characteristics (Fig. 1): flattened morphology, pronounced decrease in DNA synthesis and intense senescence-associated β-Galactosidase (SA-β-Gal) staining, elevated levels of cell cycle inhibitors CDKN1A (p21), CDKN2A (p16), and CDKN2B (p15), and diminished HMGB11 and LAMINB1 protein levels. Following 20 d in senescence, however, the senescent *Atm*−/− cultures displayed regrowth signs (*SI Appendix*, Fig. S2), which was reminiscent of the postcrisis resurgence of WT MEFs (34, 36), indicating escape from senescence or selection for senescence-resistant cells. Importantly, at P8, the average telomere length of senescent *Atm*−/− fibroblasts was comparable to that of proliferating WT fibroblasts (*SI Appendix*, Fig. S4), suggesting that telomere erosion was not a significant factor in their rapid senescence and pointing to alternative mechanisms driving this process. Notably, the accelerated senescence of murine *Atm*−/− lung fibroblasts

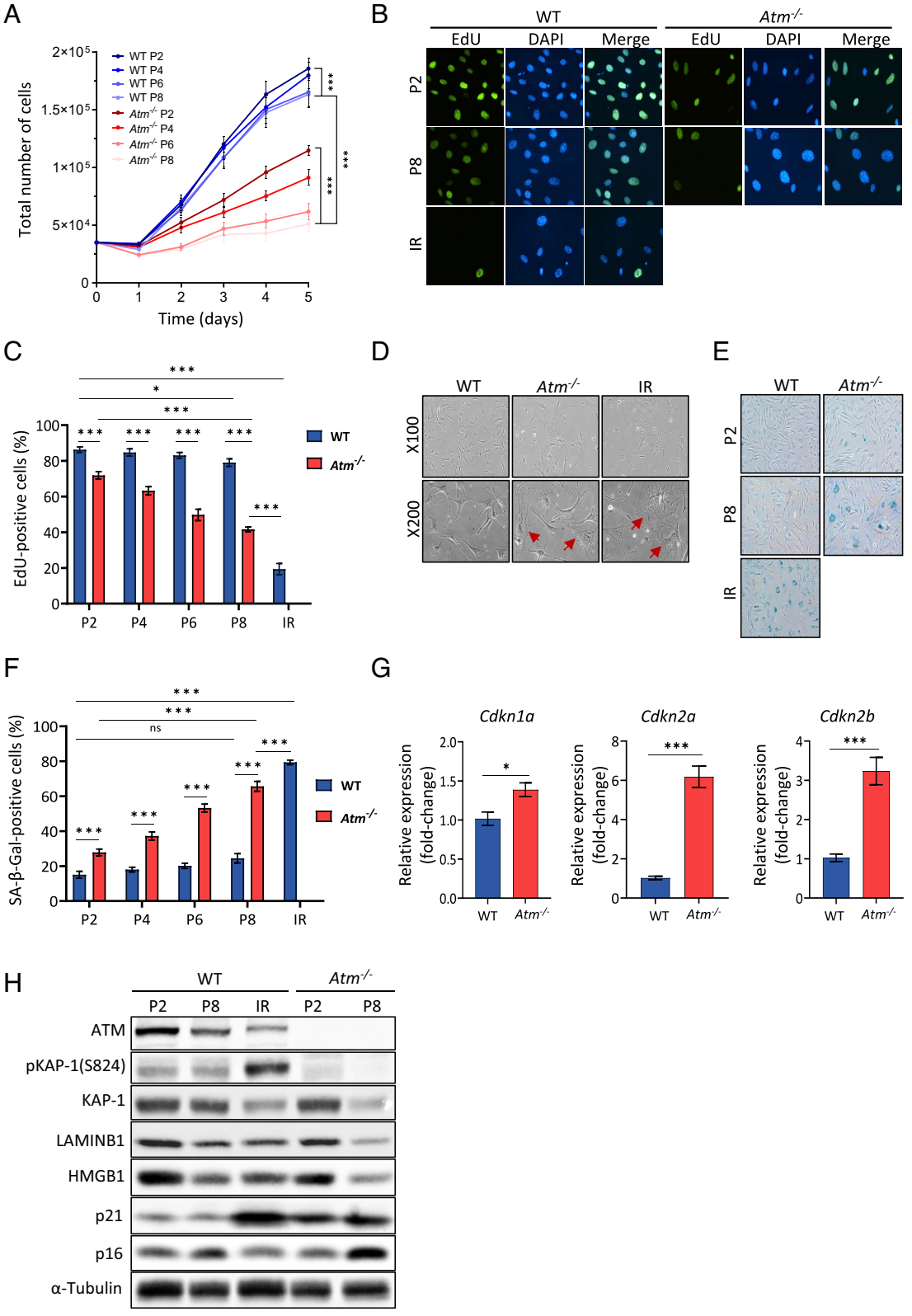

Fig. 1. Premature senescence in murine *Atm*−/− lung fibroblasts at 3% O_2 concentration. (*A*) Growth curves of WT and *Atm*−/− cells across passage levels P2 to P8. (*B*) Representative EdU staining images of WT and *Atm*−/− cells at P2 and P8 (EdU: green; nuclei: blue). (*C*) Quantification of EdU-positive cells for WT and *Atm*−/− cells at various passage levels (P2 to P8). IR denotes WT cells exposed to 10 Gy of ionizing radiation and analyzed 10 d postexposure. (*D*) Bright-field microscopy images of cells at P8, with red arrows indicating cells exhibiting senescent morphology. (*E*) SA-β-Gal activity staining in cells at P2 and P8. (*F*) Quantitative analysis of SA-β-Gal-positive cells at different passage levels. (*G*) RT-qPCR analysis of cell cycle arrest mediators' genes at P8. (*H*) Western blotting analysis of senescence-associated markers in WT and *Atm*−/− cells at P2 and P8, along with irradiated WT controls. Data in panels *C*, *F*, and *G* are represented as mean + SEM from at least three independent experiments. Statistical significance determined using a two-tailed *t* test is denoted as follows: **P* < 0.05, ****P* < 0.0̄01, and ns = not significant.

occurred earlier and more rapidly than that of human A-T skin fibroblasts grown under identical conditions (13), whereas murine WT lung fibroblasts never senesced, unlike human control skin fibroblasts. Therefore, the contrast between ATM-proficient and -deficient cells was starkly more evident in the murine cell system than in the human one.

Marked Genome Instability in *Atm*−/− Lung Fibroblasts under Physiological Oxygen Conditions. Genome instability is a defining feature of A-T. Given the markedly accelerated senescence of *Atm*−/− mouse lung fibroblasts relative to human A-T fibroblasts, we evaluated the extent of genome instability in these cells. We noted increased DNA damage in *Atm*−/− fibroblasts, evidenced by elevated levels of γH2AX foci and the presence of MN, starting from early passages (*SI Appendix*, Fig. S5 *A* and *B*). Similarly, cytogenetic analyses revealed pronounced chromosomal aneuploidy and breakage from the outset (*SI Appendix*, Fig. S5 *C–E*), indicating that these cells inherently exhibit significant genome instability, which predates the manifestation of senescence. Interestingly, we observed a rise in aneuploidy and polyploidy as cells neared senescence, as shown by chromosome counts (*SI Appendix*, Fig. S5*D*) and low-pass whole genome sequencing (LP-WGS) (*SI Appendix*, Fig. S5*F*). Notably, as cytogenetic analysis is based on proliferating cells, the metaphases observed in *Atm*−/− cultures at P8 were likely derived from cells that retained the ability to divide, despite the predominant senescence in *Atm*−/− fibroblasts at this stage.

Dynamic Induction of Senescence through Loss of ATM Protein or Inactivation of Its Catalytic Activity. The *Atm*−/− genotype creates mice deficient in ATM from the outset, linking the resulting phenotype to the absence of ATM protein. Genetic manipulations in mice allow, however, the induction of such genotype in specific tissues postnatally, in otherwise healthy animals. We explored whether triggering *Atm* gene inactivation in ATM-proficient lung fibroblasts would prompt senescence, a state these cells normally avoid under 3% oxygen conditions. We utilized lung fibroblast lines from a mouse strain previously engineered in our lab (37), homozygous for a "floxed" *Atm* allele (38, 39) and carrying a Cre(ERT)-expressing transgene. Cre(ERT) is designed to remain cytoplasmic, relocating to the nucleus after 4-hydroxytamoxifen (4-OHT) exposure (40). As expected, these ATM-proficient fibroblasts initially proliferated robustly, like WT cells. Yet, upon 4-OHT treatment and presumed homozygous *Atm* inactivation, ATM protein levels decreased in these cells within four days to almost undetectable levels (*SI Appendix*, Fig. S6 *A* and *B*), aligning with ATM's 20 to 24 h half-life in cultured cells. Ten days later, cellular proliferation halted, and the cells exhibited senescence markers, mirroring senescent *Atm*−/− cells (*SI Appendix*, Fig. S6 *C–E*). Accordingly, these cells exhibited elevated numbers of γH2AX foci and MN (*SI Appendix*, Fig. S6 *F* and *G*). This result highlights the essential role of ATM in maintaining continuous proliferation and preventing genome instability and senescence in murine lung fibroblasts growing under physiological oxygen concentration.

We asked whether inhibition of ATM kinase activity without protein elimination could induce senescence in WT cells. The ATM inhibitor, KU-60019 (41) (ATMi hereafter), efficiently and reversibly blocks ATM kinase activity (*SI Appendix*, Fig. S7). We noticed that the inhibitor retained its potency for at least 6 d in culture (*SI Appendix*, Fig. S7 *A* and *B*), facilitating its use for extended ATM inhibition in cell culture. Importantly, unlike irreversible *Atm* gene excision, the reversibility of ATM's chemical inhibition upon the inhibitor's removal allows for the withdrawal of the senescence stimulus after its induction (*SI Appendix*, Fig. S7*C*). Indeed, after 15 d in the presence of ATMi, WT lung fibroblasts ceased proliferation and the cultures displayed senescence hallmarks (*SI Appendix*, Fig. S8), mirroring the characteristics of senescent *Atm*−/− cells (Fig. 1). However, when ATMi was subsequently removed, this ATMi-induced senescence state was reversed (*SI Appendix*, Fig. S9 *A–D*), with a concomitant decline in the levels of γH2AX foci and MN back to normal (*SI Appendix*, Fig. S9 *E* and *F*). This finding suggests that the loss of ATM's catalytic activity alone is sufficient to induce genome instability and senescence in lung fibroblasts. Furthermore, this system may offer a tool for dynamically modulating senescence in WT primary fibroblast cultures. However, it should be cautiously noted that some cells with inactivated ATM may not have fully entered senescence and could resume proliferation more readily than others after the inhibitor's removal.

Loss of p53 Increases Genome Instability in *Atm*−/− Lung Fibroblasts and Facilitates Senescence Evasion, Which Ultimately Leads to Tumorigenicity. The tumor suppressor protein, p53, is pivotal in initiating and sustaining the cell cycle checkpoints induced by DNA lesions, a process that can lead to cellular senescence in response to prolonged induction of DNA damage (42). Senescing *Atm*−/− cells exhibited increased expression of the *Cdkn1a* gene, a crucial target of p53 in this context, and consequently, an elevated level of its protein product, p21 (Fig. 1 *G* and *H*). This finding suggests p53's involvement in the pathway leading to this senescence, despite the absence of Atm, which is a primary p53 activator in the DSB response (7, 8). We therefore asked whether lung fibroblasts deficient in both ATM and p53 might bypass the ATM deficiency-induced senescence. We attempted to generate *Atm*- and *Trp53*-double-knockout (dKO) mice by breeding C57BL animals heterozygous for null alleles of both genes. However, these dKOs typically arise at extremely low sub-Mendelian frequencies (43), making it challenging to obtain them. After genotyping 719 offspring without identifying a single dKO, we shifted our focus to the more prevalent *Atm*−/−;*Trp53*+/− genotype, asking whether a partial reduction in p53 levels could still impact the senescence dynamics associated with ATM deficiency.

Initially, the *Atm*−/−;*Trp53*+/− genotype did not enhance the slow growth and low DNA synthesis typical of ATM-deficient cells, and cells with this genotype exhibited elevated SA-β-Gal staining (Fig. 2 *A–C*). However, as these cells advanced in passage levels, the proportion of SA-β-Gal-positive cells dropped rapidly, the cultures did not enter senescence, and rather than stalling at P8, their growth was accelerated, eventually surpassing the WT rate at P15, and their SA-β-Gal staining disappeared (Fig. 2 *A–C*). Interestingly, while this genotype did exhibit at P8 the alterations in specific protein levels that characterize senescent *Atm*−/− cells, this trend was reversed at P15 (Fig. 2*D*), further attesting to senescence evasion. We suspected that the cultures evaded senescence due to gradual loss-of-heterozygosity (LOH) at the *Trp53* locus, which eventually rendered the cells dKO for *Atm* and *Trp53*. Subsequent genotyping of the cells across various passage levels confirmed this assumption, revealing a progressive loss of the WT *Trp53* allele in the cultures, which correlated with the acceleration in cellular proliferation (Fig. 2 *A* and *B*). Notably, with extended culturing, LOH was also detected in *Atm*+/+;*Trp53*+/− cells, albeit at considerably higher passage levels compared to *Atm*−/−;*Trp53*+/− cells (*SI Appendix*, Fig. S10*A*). These observations suggest that LOH at the *Trp53* locus was expedited in the context of ATM deficiency, likely due to the increased genome instability associated with ATM absence.

To further establish p53's involvement in the premature senescence of ATM-deficient cells, we examined the effect of ATMi on lung fibroblast lines derived from *Trp53*−/− mice. Unlike WT

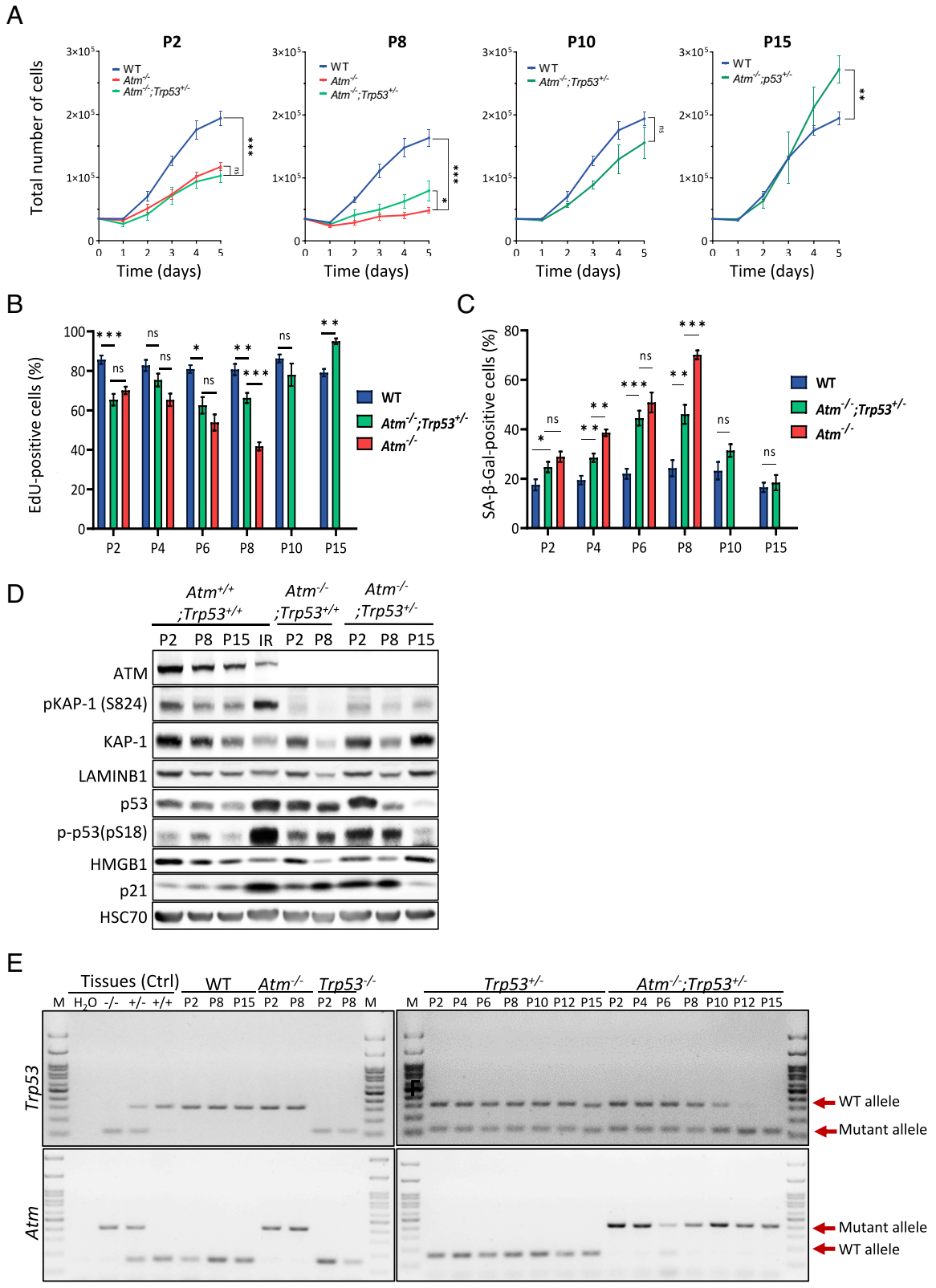

Fig. 2. p53 loss leads to early senescence escape in ATM-deficient murine lung fibroblasts. (*A*) Growth curves of cells with different *Atm/Trp53* genotypes at different passage levels. (*B*) Quantification of EdU in cells with different *Atm/Trp53* genotypes at different passage levels (P2 to P15). (*C*) Quantification of SA-β-Gal in cells with the different *Trp53/Atm* genotypes at different passage levels (P2 to P15). (*D*) WB analysis of cell cycle arrest and senescence markers in cells with different *Atm/Trp53* genotypes at P2, P8, and P15. (*E*) PCR analysis of *Trp53* (*Upper*) and *Atm* (*Lower*) alleles in cells with the different *Atm/Trp53* genotypes at different passage levels. Note that by P15, the cells with the initial genotype, *Atm−/−;Trp53+/−*, were already dKO. Mean and SEM of at least three independent experiments are shown. *P*-values were calculated using the two-tailed *t* test (**P* < 0.05, ***P* < 0.01, ****P* < 0.001, ns = not significant).

cells, continuous exposure to ATMi did not induce growth arrest or senescence hallmarks in *Trp53−/−* cells (*SI Appendix*, Fig. S11 *A* and *B*), suggesting once again that the absence or inactivity of ATM does not precipitate a senescence state without the involvement of p53. Consistent with expectations, *Trp53−/−* cells exposed to ATMi displayed elevated levels of γH2AX foci (*SI Appendix*,

Fig. S11*C*) and MN (*SI Appendix*, Fig. S11*D*), indicative of increased genome instability.

The simultaneous absence of both ATM and p53 calls for excessive genome instability. Indeed, genome stability was heightened in dKO cells compared to *Atm*−/− cells that underwent spontaneous senescence escape. The elevation was evident in the amounts of γH2AX foci and MN (*SI Appendix*, Fig. S12 *A* and *B*), as well as in chromosomal aneuploidy and polyploidy observed through cytogenetic analysis (*SI Appendix*, Fig. S12*C*) or LP-WGS (*SI Appendix*, Fig. S12*D*). Notably, the chromosomal instability in dKO cells also surpassed that of *Trp53*−/− cells (*SI Appendix*, Fig. S12 *C* and *D*). Upon further proliferation, at P35, genome instability continued to escalate across the various genotypes (*SI Appendix*, Fig. S10 *B*–*D*). Remarkably, at this stage, these cell lines demonstrated robust proliferation under ambient oxygen conditions (*SI Appendix*, Fig. S13), which normally leads to rapid senescence of WT lung fibroblasts (*SI Appendix*, Fig. S1).

Collectively, these cells exhibited characteristics consistent with immortalization, prompting us to investigate whether they had progressed to a tumorigenic state. Indeed, following subcutaneous injection into nude mice and a latency period of approximately 4 wk, both WT and *Atm*−/−;*Trp53*−/− cells at P35 formed tumors in the animals (*SI Appendix*, Fig. S14). The acquisition of tumorigenic potential by the WT cells is particularly notable, as these cells underwent no directed manipulation and developed this potential after a relatively short period of growth under 3% oxygen. Notably, at this high passage level, the p53 pathway was down-regulated as reflected by reduced mRNA and protein levels of two p53 target genes, *Cdkn1a* and *Mdm2* (*SI Appendix*, Fig. S15). Interestingly, the protein levels of p53 itself remained high (*SI Appendix*, Fig. S15), suggesting that its function may have been impaired due to *Trp53* mutations that occurred during the progression of these cells in culture.

Atm−/− Lung Fibroblasts Display Persistent Upregulation of ISGs. In our recent investigation into the accelerated senescence in skin fibroblast lines derived from A-T patients (13), we noticed an elevated expression of ISGs in senescing A-T cells, likely indicating activation of the cGAS–STING pathway by cytoplasmic DNA emanating from ruptured MN (44). In the present study, we further explored the signaling underlying this process. We employed transcriptomic analysis using RNA-seq on three WT and three *Atm*−/− murine lung fibroblast lines sampled at P2 (early growth) and P8, the stage at which *Atm*−/− cells reached senescence. A total of 15,389 mRNA transcripts were represented in these samples. Principal Component Analysis (PCA) indicated a strong correlation between replicate samples, suggesting that the most robust gene signatures were primarily driven by the experimental conditions rather than other confounding factors (*SI Appendix*, Fig. S16*A*).

We also examined WT cells that underwent senescence upon exposure to ATMi, subsequently sampling them again after they resumed normal proliferation following inhibitor removal. PCA based on 15,372 expressed genes, revealed that the experimental conditions had the most significant impact on gene signatures, with the primary effect caused by ATM inhibition and its subsequent release (*SI Appendix*, Fig. S16*B*).

To identify the differentially expressed genes (DEGs) associated with premature senescence due to ATM deficiency, we conducted multiple comparison tests based on genotype and passage levels, including an interaction comparison (*Materials and Methods*). This analysis yielded a total of 2,163 DEGs across the different groups (*SI Appendix*, Table S1). We then applied a separation test after each comparison to retain only the genes that showed consistent responses across the corresponding replicates for subsequent analyses. Ultimately, 2,123 DEGs were significantly up- or down-regulated in senescent cells (*SI Appendix*, Table S1).

Notably, as observed in senescent human A-T cells, we detected a widespread activation of ISGs, particularly those responsive to IFN-α (Fig. 3 *A* and *B* and *SI Appendix*, Fig. S17). Importantly, the majority of up-regulated ISGs exhibited elevated expression levels in *Atm*−/− cells at early passages, and this elevation persisted until the cells reached senescence (Fig. 3*B*), suggesting a sustained activation of the IFN response in these cells from the outset. Among the prominently induced classical ISGs was *Irf7* (Fig. 3*B* and *SI Appendix*, Fig. S17), which encodes a master regulator of type I IFN production, and other ISGs that encode SASP components, such as IGFBP6, CCL7, VCAM1, and CSF1 (Fig. 3*B*). Crucially, a similar ISG response was observed in WT cells undergoing senescence due to exposure to ATMi (Fig. 3 *C* and *D*). Furthermore, upon ATMi removal and subsequent reversal of senescence, the expression levels of the majority of ISGs decreased to normal levels (Fig. 3*C*). This observation indicates that the senescence state observed in WT cells exposed to ATMi shared similar characteristics with that of *Atm*−/− cells. Furthermore, it suggests that this IFN response is an integral component of the accelerated senescence observed in ATM-deficient fibroblasts.

Remarkably, our RNA-seq analysis did not reveal detectable levels of the interferon genes themselves. However, considering that even minute quantities of IFNs can induce the production of ISGs (45), we employed RT-qPCR to specifically detect the transcripts of individual IFNs. Intriguingly, expression of *Ifna1* was elevated in *Atm*−/− cells compared to WT cells (*SI Appendix*, Fig. S17), whereas transcripts encoding IFNβ1 and IFNγ were still undetectable by this method, same as IFNα2, and IFNα4 of the IFNα family. These findings suggest that, at least IFNα1 might be generated in senescing *Atm*−/− cells at levels sufficient to trigger the observed downstream ISG expression.

Chemical Inhibition of cGAS Enables Senescence Evasion in _Atm_−/− Lung Fibroblasts. The combination of genome instability leading to MN formation, IFN response, and eventual senescence observed in both human A-T fibroblasts (13) and mouse *Atm*−/− fibroblasts (this study) suggests the involvement of the innate immunity cGAS–STING pathway (46) as a signaling axis in the accelerated senescence resulting from ATM absence. A hallmark of genome instability, MN eventually rupture, releasing dsDNA into the cytoplasm (47). Cytoplasmic DNA, in turn, acts as a prime activator of the cGAS–STING pathway, ultimately leading to upregulation of interferon genes and subsequently, ISGs. This pathway has been tightly associated with cellular senescence in various experimental setups (44, 48).

Indeed, in the presence of cGAS and STING inhibitors, RU.521 and H151 (referred to as cGASi and STINGi) (49, 50), *Atm*−/− fibroblasts bypassed arrest at P8 (Fig. 4*A*) and exhibited reduced SA-β-Gal staining compared to untreated controls (Fig. 4*B*). Furthermore, p16, $p21^{Wai1/CiP1}$, and p15 levels along with *Ifna1* expression were lowered in cGASi-treated *Atm*−/− cells (*SI Appendix*, Fig. S18*A*), suggesting evasion of spontaneous senescence. Notably, after cGASi removal, these cells continued to proliferate without entering senescence (*SI Appendix*, Fig. S19 *A* and *B*), while displaying elevated genome instability (*SI Appendix*, Fig. S19 *C* and *D*). This observation suggests that ATM-deficient fibroblasts that bypass the time window for spontaneous senescence, are unlikely to undergo this process at a later stage.

Notably, cGASi and STINGi treated *Atm*−/− fibroblasts also displayed reduced numbers of γH2AX nuclear foci and percentage of MN-positive cells during treatment with the inhibitors (Fig. 4 *C* and *D* and *SI Appendix*, Fig. S18 *B* and *C*). cGASi

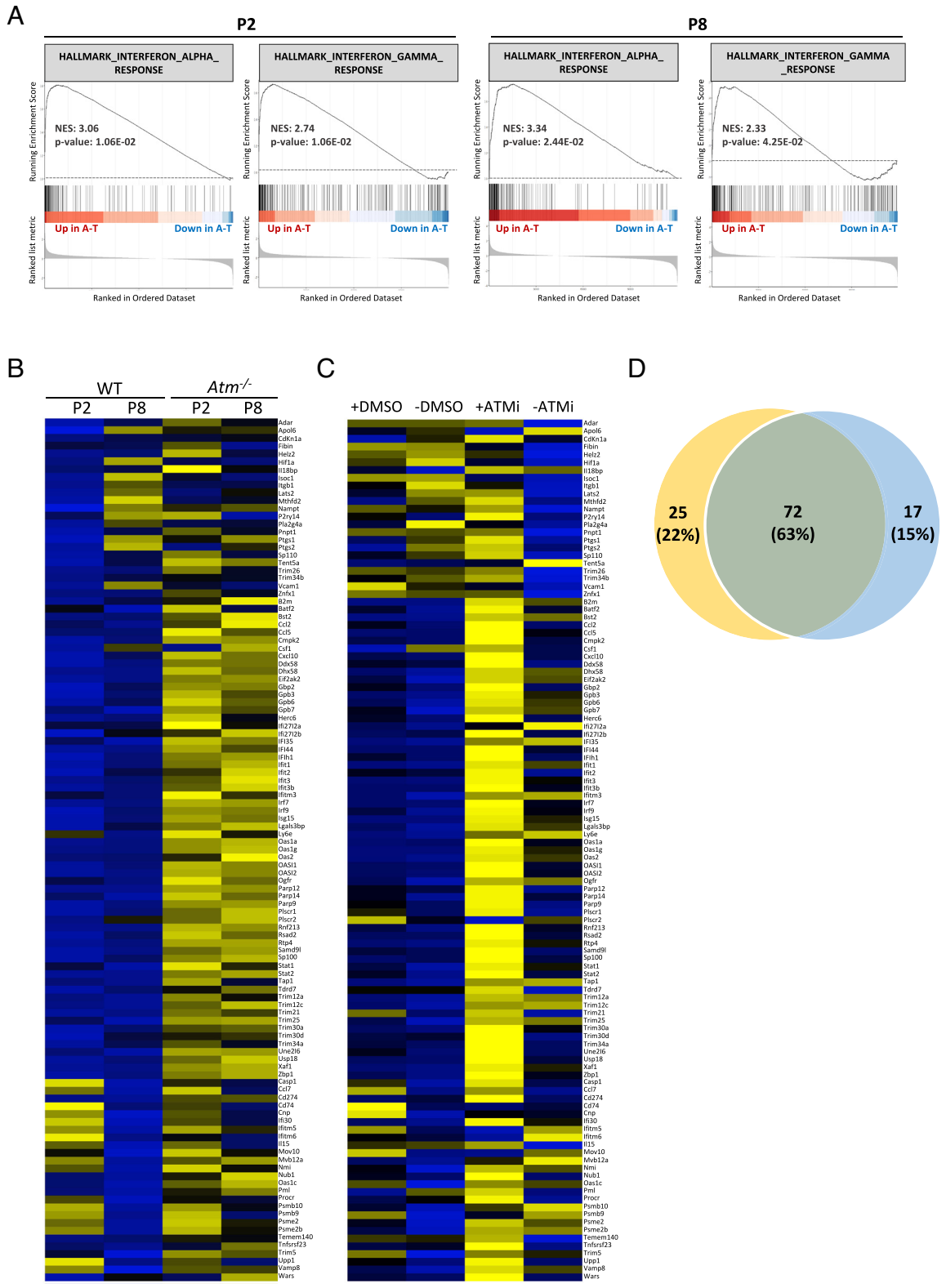

Fig. 3. *Atm*−/− lung fibroblasts exhibit high, sustained expression of ISGs. (*A*) GSEA plots for hallmark interferon gene sets when global gene expression was compared between *Atm*−/− and WT cells at P2 (*Upper*) and P8 (*Lower*). (*B*) A representative heat map of IFN response genes in *Atm*−/− and WT cells at P2 and P8. Blue represents downregulation, and yellow–upregulation. (*C*) Representative heat map of IFN-response genes in WT cells following treatment with ATMi (+ATMi) or DMSO (+DMSO) for 15 d, and 20 d after ATMi (−ATMi) or DMSO removal (−DMSO). Blue represents downregulation and yellow–upregulation. (*D*) Venn diagram of up-regulated ISGs in both datasets (yellow; up-regulated genes in *Atm*−/− cells, blue; up-regulated genes in WT cells during ATMi treatment). The overlap represents ISGs that were up-regulated in both setups. The upregulation in *Atm*−/− cells at P8 is compared to WT cells at P8, and in WT cells the comparison is between cells treated with ATMi and those treated with DMSO.

slightly reduced chromosomal polyploidy compared to cells untreated with the inhibitor, although it was clear that in the presence of cGASi, they still exhibited genome instability (*SI Appendix*, Fig. S18 *D–F*). Collectively, these results support the notion of a pivotal role for cGAS in the premature senescence of *Atm*−/− fibroblasts.

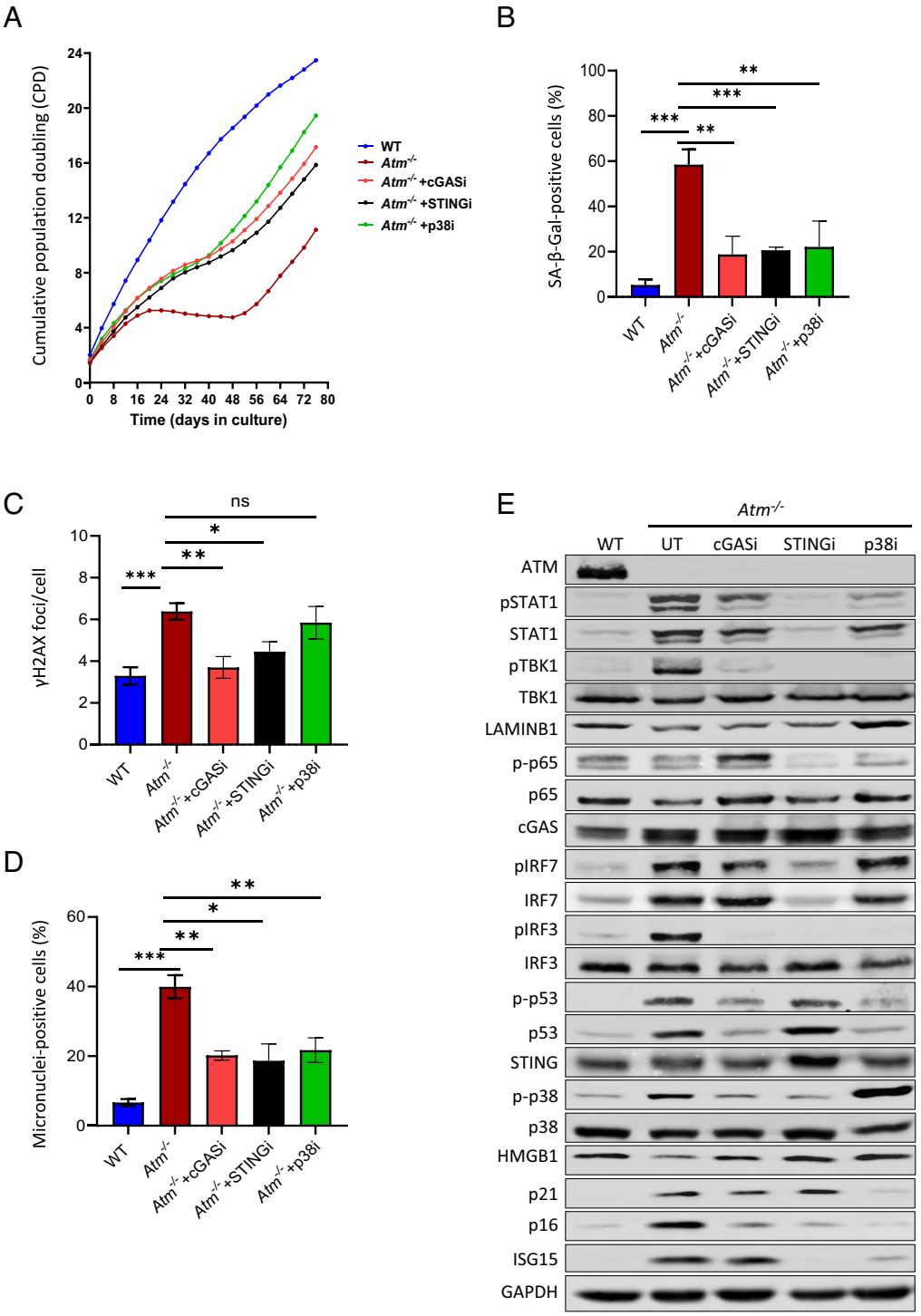

Fig. 4. The p38 MAPK is a major regulator of the premature senescence of *Atm*−/− lung fibroblasts. (*A*) CPD curves of WT and *Atm*−/− cells cultured in the presence with cGASi, STINGi, and p38i. (*B*) Quantification of the percentage of SA-β-Gal-positive cells from figure (*A*) at P.8 (day 32). (*C*) Quantification of average γH2AX nuclear foci per cell from (*A*) at P8. (*D*) Quantification of MN in cells from experiment (*A*) at P8. A cell was considered micronuclei-positive if it contained at least one micronucleus. (*E*) WB analysis of various IFN-related proteins, senescence markers, and cell cycle arrest mediators in cellular extracts from cells in experiment (*A*), at P8. Mean and SEM of at least three independent experiments are shown. *P*-values were calculated using the unpaired *t* test (**P* < 0.05, ****P* < 0. 01, ****P* < 0.001, ns = not significant).

p38 MAPK Collaborates with cGAS and STING to Mediate Premature Senescence in *Atm*−/− Lung Fibroblasts. The cGAS–STING–IFN axis functionally interacts with other signaling pathways (44, 48). The p38 MAP kinase (MAPK) route is involved in mediating the antiproliferative effects of Type I IFNs, and the role of p38 in cellular senescence, triggered by various stimuli, is well established (51). Furthermore, phosphorylation of p38 was previously shown in skin fibroblasts from A-T patients, and knocking down the *MAPK14* gene encoding p38 prevented their premature senescence (52).

Similar to cGASi and the STING inhibitor (STINGi), a p38 inhibitor (p38i) facilitated evasion of senescence in *Atm*−/− cells: It increased their proliferation rate, prevented senescence-associated growth arrest, and decreased the number of SA-β-Gal-positive cells, potentially enabling their eventual immortalization (Fig. 4 *A* and *B*). Although p38i did not significantly reduce γH2AX foci

levels, it significantly decreased MN formation, similar to STINGi and cGASi (Fig. 4 *C* and *D*). Importantly, similarly to human A-T fibroblasts (52), senescing *Atm*−/− cells exhibited increased p38 phosphorylation, which was attenuated by both cGASi and STINGi (Fig. 4*E*). Interestingly, p38 phosphorylation was increased in the presence of p38i, and STINGi treatment led to increased STING level (Fig. 4*E*), suggesting feedback mechanisms that attempt to activate or increase the amount of these proteins in response to their chemical inhibition.

Like cGASi, p38i reduced the levels of p53, p21, and p16 and reversed other senescence markers such as HMGB1 and LAMINB1 levels (Fig. 4*E*). In contrast, STINGi did not affect p53 and p21 levels, suggesting that STING might be involved in the premature senescence of *Atm*−/− cells mainly through p16. Surprisingly, inhibition of p38 also diminished the phosphorylation of the downstream effectors of cGAS–STING, TBK1, and IRF3 (Fig. 4*E*), raising the possibility that p38, in addition to its role in mediating cell cycle arrest, might also contribute to the enhancement of interferon signaling in these cells upon activation.

The cGAS–STING pathway interacts with the JAK-STAT pathway, implicated in ISG activation (53). We observed in *Atm*−/− cells high levels of STAT1 and its phosphorylated forms (Fig. 4*E*). Unlike the effects seen with STINGi, the inhibition of cGAS only minimally affected the phosphorylation of STAT1 and the expression of ISGs, including *Isg15*, *Irf7*, and *Stat1* (Fig. 4*E*). This suggests that, even in the absence of cGAS activity, other DNA damage sensors might still activate STING, maintaining high ISG expression in *Atm*−/− cells. Additionally, the levels of the p65 subunit of NF-κB and its phosphorylated form were not elevated in *Atm*−/− compared to WT cells (Fig. 4*E*). This finding aligns with our previous observations in senescing A-T skin fibroblasts under 3% O_2 (54). Collectively, the data indicate a signaling loop activated by genome instability, driven by a tight cross talk between the cGAS–STING, p38, and p53 pathways (Fig. 5).

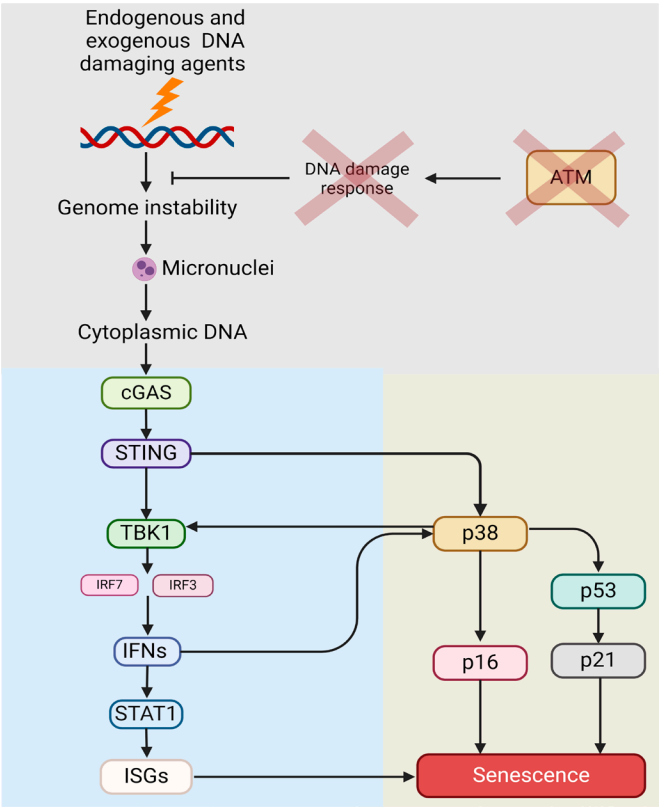

Fig. 5. Model depicting cellular pathways involved in premature senescence of ATM-deficient lung fibroblasts. Persistent genome instability, coupled with ongoing DNA damage, leads to MN formation and the release of nuclear DNA into the cytoplasm. Central to this process is the signaling cascade that begins with the activation of cGAS and STING, ultimately leading to the activation of IFN genes and downstream ISGs. The model also considers potential additional nuances, such as STING activation by other triggers and cross talk with the p38 MAPK and p53 pathways. Collectively, this network halts cell cycle progression and activates various features of senescence, most notably the SASP. Figure created with BioRender.

Discussion

Our experiments demonstrate that the growth patterns of WT murine lung fibroblasts closely resemble those of MEFs (34): Both cell types exhibit rapid senescence under ambient oxygen levels and indefinite growth under 3% oxygen. However, this robust growth is replaced by rapid senescence when ATM is absent or inhibited. This difference between WT and ATM-deficient murine lung fibroblasts is more profound than the difference observed between human skin fibroblasts derived from A-T patients and controls (11, 13). Notably, unlike in human A-T fibroblasts, telomere attrition does not contribute to the rapid senescence of murine *Atm*−/− lung fibroblasts, as murine telomeres are significantly longer. Instead, their rapid senescence can be attributed primarily to the marked genome instability that we observed in these cells (Fig. 5).

The cell cycle arrest in senescent cells is commonly considered irreversible (55). However, recent studies have shown that senescent cells can resume cycling under certain circumstances, particularly tumor cells that have become senescent following therapeutic treatments (reviewed in ref. 56). In this study, we observed instances of the dynamics of senescence states resulting from the absence of the ATM protein or its catalytic activity. Specifically, senescent *Atm*−/− cells eventually escaped senescence, acquiring accelerated proliferation, marked genome instability, and even insensitivity to ambient O_2 levels. In contrast to senescence escape, senescence reversal is a distinct phenomenon where the cell reverts to its presenescent state after senescence-associated growth arrest, regaining its original structure and function (57). Our study shows that WT murine lung fibroblasts can resume proliferation following temporary ATMi-induced senescence state. Upon ATMi removal, the proliferation rates of the cells returned to normal, and the numbers of γH2AX foci and MN were markedly reduced, indicating that the ATMi-induced senescence state involved intrinsic DNA damage and was dynamic and potentially reversible. Importantly, the gene expression patterns during this senescence state were similar to those of senescent *Atm*−/− cells, suggesting that despite being temporary and potentially reversible, this senescence state was similar to that induced by ATM absence.

These findings add another dimension to the potentially detrimental impact of senescent cells accumulating during cancer therapy, particularly if these cells later resume proliferation. Given their origin as tumor cells and augmented genome instability caused by marked repression of DNA repair pathways (Frey et al., in press), (58) this phenomenon may partly account for the highly aggressive and treatment-resistant nature of tumors that recur after escaping therapy-induced senescence (56).

High levels of p53 and $p21^{CiP1/Waf1}$ were observed in senescing *Atm*−/− cells, suggesting that the p53 pathway is preserved in these cells. Notably, $p21^{CiP1/Waf1}$ levels in *Atm*−/− cells were constitutively higher than normal, even at early passage levels. This may explain, at least in part, why *Atm*−/− cells grew slowly immediately after culture setup. Furthermore, we showed that the loss of p53 allowed *Atm*−/− cells to evade senescence, leading to early immortalization, robust growth, and extensive genome instability. Our findings align with previous observations in MEFs, which demonstrated that already at early passages, *Atm*−/−; *Cdkn1a*−/−, and

Atm−/−;*Trp53*−/− MEFs proliferate similarly to WT MEFs and are capable of proliferating at higher passages compared to *Atm*−/− cells, which proliferate slowly and senesce rapidly (59, 60). Finally, we show that inhibition of ATM kinase activity in p53-deficient cells failed to induce senescence. Altogether, these results suggest that the p53/p21 axis is central to cellular senescence caused by ATM absence. Notably, unlike $p21^{Cip1/Waf1}$, the levels of $p16^{INK4A}$ increased in *Atm*−/− fibroblasts only at later passage levels, when the cells were entering senescence. This suggests that the p53/$p21^{Cip1/Waf1}$ axis might play a role in initiating the cell cycle arrest while $p16^{INK4A}$ is required for maintenance of the senescence-associated growth arrest (61).

Our results indicate that murine WT lung fibroblasts grown under 3% O_2 eventually become immortalized, similarly to MEFs growing under this oxygen concentration (34, 35). Furthermore, these fibroblasts acquire tumorigenic potential without any external manipulation. This finding suggests a caution in using these cells as a primary cell system, which should probably be limited to early passage levels. However, these cells also provide a convenient experimental system for studying the genomic alterations that drive the neoplastic transformation of primary diploid cells. Notably, both WT and genomically unstable *Atm*−/−;*Trp53*−/− cells eventually acquired the tumorigenic potential, making the sequence alterations driving this process in WT cells particularly intriguing. A key suspect in this regard is the p53 pathway, and indeed, we observed a marked decrease in readouts of the p53 pathway in WT fibroblasts at the stage when they became neoplastic. The combination of chromosomal instability and reduced p53 pathway activity likely paved the way for malignant transformation.

We demonstrate a robust activation of the IFN pathway, particularly the IFNα-associated response, in senescing *Atm*−/− lung fibroblasts. This activation is highlighted by the high expression of *Ifna1* and downstream ISGs, including *Irf7*, which encodes a transcription factor that regulates *Ifna* itself (62). The elevated expression of these ISGs in WT cells undergoing senescence under ATMi treatment, and their subsequent downregulation following ATMi removal and reversal of senescence, strongly links the IFN response to the rapid senescence associated with ATM absence. Notably, the expression of genes encoding other interferons, such as IFNγ and IFNβ, was not detected. Additionally, the NF-κB signaling pathway was down-regulated in senescent *Atm*−/− fibroblasts, similar to our previous observations in senescent human A-T fibroblasts (54). These findings suggest that the signaling loop driving the senescence of *Atm*−/− fibroblasts (Fig. 5) culminates in the activation of the Ifnα axis.

Inhibition of cGAS alleviated the pronounced senescence of *Atm*−/− fibroblasts yet had only a minor effect on ISG expression. This led us to suggest a possible cGAS-independent role for STING in this process. Confirming this suggestion, inhibiting STING activity not only rescued the senescence of *Atm*−/− cells, similar to cGAS inhibition, but also significantly reduced the IFN response. Notably, cGAS and STING have recently been reported to exhibit independent activities or different modes of action in various contexts (63–65).

These observations are consistent with previous studies demonstrating the involvement of the cGAS–STING pathway in the premature senescence of *ATM*−/− brain organoids (66), as well as its activation following ATM inhibition or depletion in murine cancer cells (67).

The p38 pathway is known to mediate the antiproliferative effects of type I IFNs and has been implicated in cellular senescence (68), specifically in the SASP (69) and in activating the p53/$p21^{Waf1/Cip1}$ axis in response to oxidative stress (70). Importantly, both cGASi and STINGi treatments reduced p-p38 levels, suggesting that p38 functionally interacts with the cGAS–STING pathway in this context. p38i, which allowed *Atm*−/− cells to evade senescence, also diminished the activity of the p53/p21 axis and the IFN response. This indicates a cross talk between the p38 and cGAS–STING pathways, with p38 amplifying the IFN response (Fig. 5).

In conclusion, our study underscores the critical role of the innate DNA sensing pathway in regulating the accelerated cellular senescence in *Atm*−/− lung fibroblasts. In the absence of ATM in these cells, a cross talk between this pathway and the p38 and p53 signaling pathways drives senescence (Fig. 5), functioning to mitigate the harmful effects of genome instability that could otherwise lead to neoplastic transformation. However, cellular senescence presents a double-edged sword, as accumulation of senescent cells in specific tissues may contribute to the segmental premature aging observed in A-T patients (9, 23). The interstitial lung disease that frequently develops in adolescent A-T patients, independent of the sinopulmonary infections (71), may exemplify this process, resembling similar conditions in aging individuals within the general population (72). Given the significant role of the cGAS–STING pathway in inflammation, senescence, and fibrotic diseases (73–75), targeting this pathway may provide new therapeutic strategies for these conditions. This idea is supported by studies demonstrating that RU.521, the cGAS inhibitor used in our study, can attenuate lung damage induced by various experimental agents in rodents (76–78) and specifically alleviate elevated senescence in cultured alveolar epithelial cells from individuals with idiopathic pulmonary fibrosis (79).

Materials and Methods

The methods in this study included the establishment and cultivation of murine lung fibroblast lines, growth curve analysis, and the assessment of cellular growth parameters, genome stability, and cell senescence. Additionally, RNA sequencing (RNA-seq) and bioinformatic analyses were performed. A detailed description of these methods and materials is available in *SI Appendix*.

Data, Materials, and Software Availability. The RNA-seq data for senescing *Atm*−/− cells are available on the GEO website under accession number GSE185673 (80), and the RNA-seq data related to chemical inhibition of ATM in WT cells are accessible under accession number GSE182731 (81).

ACKNOWLEDGMENTS. We are deeply grateful to Dr. Kenneth Hollander, Ami Nehaisy, and Abeer Saeed for their dedicated assistance in maintaining mouse colonies. Research in the Shiloh lab was supported by grants from the Dr. Miriam and Sheldon G. Adelson Medical Research Foundation (AMRF), the Horizon 2020 Marie Curie ITN "HealthAge" program (GA 812830), and the Israeli Society for Frighting A-T Disease. Work in the Ben-David lab was funded by the European Research Council (StG 945674), the Israel Cancer Research Fund, the Israel Science Foundation (grant 1805/21), and the Israel-U.S. Binational Science Foundation (grant 2019228). T.B.-Y. received a fellowship awarded by the Edmond J. Safra Center for Bioinformatics at Tel Aviv University. Research in the Tzfati lab was supported by the Israel Science Foundation (grants 2071/18 and 1342/23) and a British Council GROWTH Fellowship awarded to R.S.

Author affiliations: [a]Department of Human Molecular Genetics and Biochemistry, Faculty of Health & Medical Sciences, Tel Aviv University, Tel Aviv 69978, Israel; and [b]Department of Genetics, The Silberman Institute of Life Sciences, The Hebrew University of Jerusalem, Jerusalem 9190501, Israel

Author contributions: M.H., T.B.-Y., Y.T., U.B.-D., C.L., R.E., Y.Z., and Y.S. designed research; M.H., Y.F., A.L., A.M., T.B.-Y., R. Slutsky, and R. Smoom performed research; Y.F., A.L., A.M., T.B.-Y., R. Slutsky, R. Smoom, Y.T., U.B.-D., C.L., and R.E. contributed new reagents/analytic tools; M.H., Y.F., A.L., A.M., T.B.-Y., R. Slutsky, R. Smoom, Y.T., U.B.-D., C.L., R.E., Y.Z., and Y.S. analyzed data; and M.H., Y.F., A.L., A.M., T.B.-Y., R. Slutsky, R. Smoom, Y.T., U.B.-D., C.L., R.E., Y.Z., and Y.S. wrote the paper.

Reviewers: A.C., Technion-Israel Institute of Technology; and M.O., Weizmann Institute of Science.

The authors declare no competing interest.

1. A. M. R. Taylor *et al.*, Chromosome instability syndromes. *Nat. Rev. Dis. Primers* **5**, 64 (2019).
2. N. Chatterjee, G. C. Walker, Mechanisms of DNA damage, repair, and mutagenesis. *Environ. Mol. Mutagen* **58**, 235–263 (2017), 10.1002/em.22087.
3. V. Thada, R. A. Greenberg, Unpaved roads: How the DNA damage response navigates endogenous genotoxins. *DNA Repair (Amst)* **118**, 103383 (2022).
4. L. C. de Almeida, F. A. Calil, J. A. Machado-Neto, L. V. Costa-Lotufo, DNA damaging agents and DNA repair: From carcinogenesis to cancer therapy. *Cancer Genet.* **252–253**, 6–24 (2021).
5. C. Rothblum-Oviatt *et al.*, Ataxia telangiectasia: A review. *Orphanet. J. Rare Dis.* **11**, 159 (2016).
6. K. Savitsky *et al.*, A single ataxia telangiectasia gene with a product similar to PI-3 kinase. *Science* **268**, 1749–1753 (1995).
7. Y. Shiloh, Y. Ziv, The ATM protein kinase: Regulating the cellular response to genotoxic stress, and more. *Nat. Rev. Mol. Cell Biol.* **14**, 197–210 (2013).
8. J. H. Lee, T. T. Paull, Cellular functions of the protein kinase ATM and their relevance to human disease. *Nat. Rev. Mol. Cell Biol.* **22**, 796–814 (2021).
9. J. Aguado *et al.*, The hallmarks of aging in Ataxia-Telangiectasia. *Ageing Res. Rev.* **79**, 101653 (2022).
10. P. Amirifar, M. R. Ranjouri, R. Yazdani, H. Abolhassani, A. Aghamohammadi, Ataxia-telangiectasia: A review of clinical features and molecular pathology. *Pediatr. Allergy Immunol.* **30**, 277–288 (2019).
11. Y. Shiloh, E. Tabor, Y. Becker, Colony-forming ability of ataxia-telangiectasia skin fibroblasts is an indicator of their early senescence and increased demand for growth factors. *Exp. Cell Res.* **140**, 191–199 (1982).
12. J. A. Metcalfe *et al.*, Accelerated telomere shortening in ataxia telangiectasia. *Nat. Genet.* **13**, 350–353 (1996).
13. M. Haj *et al.*, Accelerated replicative senescence of ataxia-telangiectasia skin fibroblasts is retained at physiologic oxygen levels, with unique and common transcriptional patterns. *Aging Cell* **22**, e13869 (2023).
14. S. Banin *et al.*, Enhanced phosphorylation of p53 by ATM in response to DNA damage. *Science* **281**, 1674–1677 (1998).
15. C. E. Canman *et al.*, Activation of the ATM kinase by ionizing radiation and phosphorylation of p53. *Science* **281**, 1677–1679 (1998).
16. C. J. Bakkenist, M. B. Kastan, DNA damage activates ATM through intermolecular autophosphorylation and dimer dissociation. *Nature* **421**, 499–506 (2003).
17. S. Matsuoka *et al.*, ATM and ATR substrate analysis reveals extensive protein networks responsive to DNA damage. *Science* **316**, 1160–1166 (2007).
18. S. Schlam-Babayov *et al.*, Phosphoproteomics reveals novel modes of function and inter-relationships among PIKKs in response to genotoxic stress. *EMBO J.* **40**, e104400 (2021).
19. M. E. Graham, M. F. Lavin, S. V. Kozlov, Identification of ATM protein kinase phosphorylation sites by mass spectrometry. *Methods Mol. Biol.* **1599**, 127–144 (2017).
20. Y. Shiloh, ATM (ataxia telangiectasia mutated): Expanding roles in the DNA damage response and cellular homeostasis. *Biochem. Soc. Trans.* **29**, 661–666 (2001).
21. Y. Shiloh, H. M. Lederman, Ataxia-telangiectasia (A-T): An emerging dimension of premature ageing. *Ageing Res. Rev.* **33**, 76–88 (2017), 10.1016/j.arr.2016.05.002.
22. V. Tiwari, D. M. Wilson III, DNA damage and associated DNA repair defects in disease and premature aging. *Am. J. Hum. Genet.* **105**, 237–257 (2019).
23. Y. Shiloh, H. M. Lederman, Ataxia-telangiectasia (A-T): An emerging dimension of premature ageing. *Ageing Res. Rev.* **33**, 76–88 (2017).
24. M. Borghesan, W. M. H. Hoogaars, M. Varela-Eirin, N. Talma, M. Demaria, A senescence-centric view of aging: Implications for longevity and disease. *Trends Cell Biol.* **30**, 777–791 (2020).
25. C. López-Otín, M. A. Blasco, L. Partridge, M. Serrano, G. Kroemer, Hallmarks of aging: An expanding universe. *Cell* **186**, 243–278 (2023).
26. R. Di Micco, V. Krizhanovsky, D. Baker, F. d'Adda di Fagagna, Cellular senescence in ageing: From mechanisms to therapeutic opportunities. *Nat. Rev. Mol. Cell Biol.* **22**, 75–95 (2021).
27. C. D. Wiley, J. Campisi, The metabolic roots of senescence: Mechanisms and opportunities for intervention. *Nat. Metab.* **3**, 1290–1301 (2021).
28. L. Hayflick, P. S. Moorhead, The serial cultivation of human diploid cell strains. *Exp. Cell Res.* **25**, 585–621 (1961).
29. V. Gorgoulis *et al.*, Cellular senescence: Defining a path forward. *Cell* **179**, 813–827 (2019).
30. M. Demaria *et al.*, An essential role for senescent cells in optimal wound healing through secretion of PDGF-AA. *Dev. Cell* **31**, 722–733 (2014).
31. J. Campisi, Senescent cells, tumor suppression, and organismal aging: Good citizens, bad neighbors. *Cell* **120**, 513–522 (2005).
32. S. A. McGrath-Morrow *et al.*, Evaluation and management of pulmonary disease in ataxia–telangiectasia. *Pediatr. Pulmonol.* **45**, 847–859 (2010).
33. R. L. Chen, P. J. Wang, Y. H. Hsu, P. Y. Chang, J. S. Fang, Severe lung fibrosis after chemotherapy in a child with ataxia-telangiectasia. *J. Pediatr. Hematol. Oncol.* **24**, 77–79 (2002).
34. S. Parrinello *et al.*, Oxygen sensitivity severely limits the replicative lifespan of murine fibroblasts. *Nat. Cell Biol.* **5**, 741–747 (2003).
35. R. A. Busuttil, M. Rubio, M. E. Dolle, J. Campisi, J. Vijg, Oxygen accelerates the accumulation of mutations during the senescence and immortalization of murine cells in culture. *Aging Cell* **2**, 287–294 (2003).
36. G. J. Todaro, H. Green, Quantitative studies of the growth of mouse embryo cells in culture and their development into established lines. *J. Cell Biol.* **17**, 299–313 (1963).
37. E. Tal *et al.*, Inactive Atm abrogates DSB repair in mouse cerebellum more than does Atm loss, without causing a neurological phenotype. *DNA Repair (Amst)* **72**, 10–17 (2018).
38. S. Zha, J. Sekiguchi, J. W. Brush, C. H. Bassing, F. W. Alt, Complementary functions of ATM and H2AX in development and suppression of genomic instability. *Proc. Natl. Acad. Sci. U.S.A.* **105**, 9302–9306 (2008).
39. E. Callen *et al.*, Essential role for DNA-PKcs in DNA double-strand break repair and apoptosis in ATM-deficient lymphocytes. *Mol. Cell* **34**, 285–297 (2009).
40. J. Brocard *et al.*, Spatio-temporally controlled site-specific somatic mutagenesis in the mouse. *Proc. Natl. Acad. Sci. U.S.A.* **94**, 14559–14563 (1997).
41. S. E. Golding *et al.*, Improved ATM kinase inhibitor KU-60019 radiosensitizes glioma cells, compromises insulin, AKT and ERK prosurvival signaling, and inhibits migration and invasion. *Mol. Cancer Ther.* **8**, 2894–2902 (2009).
42. P. L. Vaddavalli, B. Schumacher, The p53 network: Cellular and systemic DNA damage responses in cancer and aging. *Trends Genet.* **38**, 598–612 (2022).
43. C. H. Westphal *et al.*, atm and p53 cooperate in apoptosis and suppression of tumorigenesis, but not in resistance to acute radiation toxicity. *Nat. Genet.* **16**, 397–401 (1997).
44. M. Motwani, S. Pesiridis, K. A. Fitzgerald, DNA sensing by the cGAS-STING pathway in health and disease. *Nat. Rev. Genet.* **20**, 657–674 (2019).
45. C. Thomas *et al.*, Structural linkage between ligand discrimination and receptor activation by type I interferons. *Cell* **146**, 621–632 (2011).
46. C. Chen, P. Xu, Cellular functions of cGAS-STING signaling. *Trends Cell Biol.* **33**, 630–648 (2023).
47. K. M. MacDonald, S. Benguerfi, S. M. Harding, Alerting the immune system to DNA damage: Micronuclei as mediators. *Essays Biochem.* **64**, 753–764 (2020).
48. C. R. R. Schmitz, R. M. Maurmann, F. Guma, M. E. Bauer, F. M. Barbe-Tuana, cGAS-STING pathway as a potential trigger of immunosenescence and inflammaging. *Front. Immunol.* **14**, 1132653 (2023).
49. J. Vincent *et al.*, Small molecule inhibition of cGAS reduces interferon expression in primary macrophages from autoimmune mice. *Nat. Commun.* **8**, 750 (2017).
50. M. Kobritz *et al.*, H151, a small molecule inhibitor of sting as a novel therapeutic in intestinal ischemia-reperfusion Injury. *Shock* **58**, 241–250 (2022).
51. A. Martinez-Limon, M. Joaquin, M. Caballero, F. Posas, E. de Nadal, The p38 pathway: From biology to cancer therapy. *Int. J. Mol. Sci.* **21**, 1913 (2020).
52. A. Barascu *et al.*, Oxidative stress induces an ATM-independent senescence pathway through p38 MAPK-mediated lamin B1 accumulation. *EMBO J.* **31**, 1080–1094 (2012).
53. R. L. Philips *et al.*, The JAK-STAT pathway at 30: Much learned, much more to do. *Cell* **185**, 3857–3876 (2022).
54. M. Haj *et al.*, Accelerated replicative senescence of ataxia-telangiectasia skin fibroblasts is retained at physiologic oxygen levels, with unique and common transcriptional patterns. *Aging Cell* **22**, e13869 (2023), 10.1111/acel.13869.
55. R. Kumari, P. Jat, Mechanisms of cellular senescence: Cell cycle arrest and senescence associated secretory phenotype. *Front Cell Dev. Biol.* **9**, 645593 (2021).
56. T. Saleh, Therapy-induced senescence is finally escapable, what is next? *Cell Cycle* **23**, 713–721 (2024), 10.1080/15384101.2024.2364579.
57. K. Evangelou, K. Belogiannis, A. Papaspyropoulos, R. Petty, V. G. Gorgoulis, Escape from senescence: Molecular basis and therapeutic ramifications. *J. Pathol.* **260**, 649–665 (2023).
58. Y. Frey, M. Haj, Y. Ziv, R. Elkon, Y. Shiloh. Broad repression of DNA repair genes in senescent cells identified by integration of transcriptomic data. *NAR*, in press.
59. Y. Xu, E. M. Yang, J. Brugarolas, T. Jacks, D. Baltimore, Involvement of p53 and p21 in cellular defects and tumorigenesis in Atm-/- mice. *Mol. Cell Biol.* **18**, 4385–4390 (1998).
60. Y. Xu, D. Baltimore, Dual roles of ATM in the cellular response to radiation and in cell growth control. *Genes. Dev.* **10**, 2401–2410 (1996).
61. M. Mijit, V. Caracciolo, A. Melillo, F. Amicarelli, A. Giordano, Role of p53 in the regulation of cellular senescence. *Biomolecules* **10**, 420 (2020).
62. K. Honda *et al.*, IRF-7 is the master regulator of type-I interferon-dependent immune responses. *Nature* **434**, 772–777 (2005).
63. Z. Cai *et al.*, cGAS suppresses beta-cell proliferation by a STING-independent but CEBPbeta-dependent mechanism. *Metab. Clin. Exp.* **157**, 155933 (2024), 10.1016/j.metabol.2024.155933.
64. J. W. Hopkins *et al.*, STING promotes homeostatic maintenance of tissues and confers longevity with aging. bioRxiv [Preprint] (2024). https://doi.org/10.1101/2024.04.04.588107 (Accessed 15 April 2024).
65. X. He *et al.*, IUPHAR ECR review: The cGAS-STING pathway: Novel functions beyond innate immune and emerging therapeutic opportunities. *Pharmacol. Res.* **201**, 107063 (2024).
66. J. Aguado *et al.*, Inhibition of the cGAS-STING pathway ameliorates the premature senescence hallmarks of Ataxia-Telangiectasia brain organoids. *Aging Cell* **20**, e13468 (2021).
67. M. Hu *et al.*, ATM inhibition enhances cancer immunotherapy by promoting mtDNA leakage and cGAS/STING activation. *J. Clin. Invest.* **131**, e139333 (2021).
68. H. Iwasa, J. Han, F. Ishikawa, Mitogen-activated protein kinase p38 defines the common senescence-signalling pathway. *Genes Cells* **8**, 131–144 (2003).
69. A. Freund, C. K. Patil, J. Campisi, p38MAPK is a novel DNA damage response-independent regulator of the senescence-associated secretory phenotype. *EMBO J.* **30**, 1536–1548 (2011).
70. J. F. Passos *et al.*, Feedback between p21 and reactive oxygen production is necessary for cell senescence. *Mol. Syst. Biol.* **6**, 347 (2010).
71. S. McGrath-Morrow *et al.*, Pulmonary function in adolescents with ataxia telangiectasia. *Pediatr. Pulmonol.* **43**, 59–66 (2008).
72. S. J. Cho, H. W. Stout-Delgado, Aging and lung disease. *Annu. Rev. Physiol.* **82**, 433–459 (2020).
73. A. Jiang, J. Liu, Y. Wang, C. Zhang, cGAS-STING signaling pathway promotes hypoxia-induced renal fibrosis by regulating PFKFB3-mediated glycolysis. *Free Radic. Biol. Med.* **208**, 516–529 (2023).
74. S. Luo *et al.*, Activation of cGAS-STING signaling pathway promotes liver fibrosis and hepatic sinusoidal microthrombosis. *Int. Immunopharmacol.* **125**, 111132 (2023).
75. J. Zhang *et al.*, The role of cGAS-STING signaling in pulmonary fibrosis and its therapeutic potential. *Front. Immunol.* **14**, 1273248 (2023).
76. R. Huang *et al.*, Inhibition of the cGAS-STING pathway attenuates lung ischemia/reperfusion injury via regulating endoplasmic reticulum stress in alveolar epithelial type II cells of rats. *J. Inflamm. Res.* **15**, 5103–5119 (2022).
77. Z. Jiang *et al.*, Inhibition of cGAS ameliorates acute lung injury triggered by zinc oxide nanoparticles. *Toxicol. Lett.* **373**, 62–75 (2023).
78. H. X. Sha *et al.*, Neutrophil extracellular traps trigger alveolar epithelial cell necroptosis through the cGAS-STING pathway during acute lung injury in mice. *Int. J. Biol. Sci.* **20**, 4713–4730 (2024).
79. M. Schuliga *et al.*, A cGAS-dependent response links DNA damage and senescence in alveolar epithelial cells: A potential drug target in IPF. *Am. J. Physiol. Lung Cell Mol. Physiol.* **321**, L859–L871 (2021).
80. M. Haj *et al.*, RNA-Seq of lung fibroblasts of Atm deficient and wildtype mice. NCBI Gene Expression Omnibus (GEO). https://www.ncbi.nlm.nih.gov/geo/query/acc.cgi?acc=GSE185673. Deposited 11 October 2021.
81. M. Haj *et al.*, Inhibition of ATM in Mouse-derived lung fibroblasts. NCBI Gene Expression Omnibus (GEO). https://www.ncbi.nlm.nih.gov/geo/query/acc.cgi?acc=GSE182731. Deposited 25 August 2021.